Density Functional Theory Study of the Manganese-Containing Ribonucleotide Reductase from *Chlamydia trachomatis*: Why Manganese Is Needed in the Active Complex

Katarina Roos* and Per E. M. Siegbahn

Department of Physics, Stockholm University, SE-106 91 Stockholm, Sweden

Received September 5, 2008; Revised Manuscript Received January 8, 2009

ABSTRACT: The active center of *Chlamydia trachomatis* (*Ct*) ribonucleotide reductase (RNR) has been studied using B3LYP hybrid density functional theory. Class Ic *Ct* RNR lacks the radical-bearing tyrosine that is crucial for activity in conventional class I (subclass a and b) RNR. Instead of the Fe(III)Fe(III)Tyr(rad) active state in conventional class I, *Ct* RNR has Mn(IV)Fe(III) at the metal center of subunit II. Based on calculated (H^+, e^-)-binding energies for *Ct* R2, iron-substituted *Ct* R2, and R2 from *Escherichia coli* (*Ec*), an explanation is proposed for why the enzyme needs this novel metal center. Mn(IV) is shown to be an equally strong oxidant as the tyrosyl radical in *Ec* R2. Fe(IV), however, is a much too strong oxidant and would therefore not be possible in the active cofactor. The structure of the catalytic center of the active state, such as protonation state and position of Mn, is discussed. *Ct* R2 has a different ligand structure than conventional class I R2 with a fourth Glu (like MMO) instead of three Glu and one Asp. Calculations indicate that, in the presence of Tyr, Glu at this position is less flexible than Asp, whereas with Phe both Glu and Asp are equally flexible. This may be a reason why conventional class I RNR has an Asp, while *Ct* R2, lacking the tyrosine, has a Glu.

Ribonucleotide reductase (RNR)[1] catalyzes the reduction of ribonucleotides to deoxyribonucleotides, the building blocks for DNA synthesis (Figure 1) (*1*). There are three classes of RNR characterized depending on their radical cofactors. Conventional class I (subclass a and b) RNR, present in, e.g., eukaryotes, consists of two subunits, R1 and R2. Reductive cleavage of molecular oxygen at a diiron metal center in R2 generates a stable tyrosyl radical. Upon substrate binding and subunit docking the radical is transferred to a cysteine in R1 more than 30 Å away via coupled proton−electron transfer through a hydrogen-bonded network (*2*−*4*). The cysteinyl radical formed initiates the substrate reaction by abstracting a hydrogen atom from the substrate 3′-carbon. After substrate reduction the radical is transferred back to the tyrosine in R2. One oxygen cleavage is enough to drive many substrate reaction cycles. The difference in proton-coupled redox potential between the tyrosine in R2 and the cysteine in R1 is crucial for activity. If it is too small, the radical cannot be transferred from R2 to R1, and if it is too large, it cannot be transferred back from R1 to R2.

At the location of the tyrosine that is essential in conventional class I RNR, the primary sequence of class Ic R2 from the human pathogen *Chlamydia trachomatis* (*Ct*) has a phenylalanine (*5*). The recently published X-ray crystal structure confirms that the phenylalanine is positioned at the position of the crucial tyrosine (*6*) (Figure 2). The *Ct* R2 active site structure also differs from conventional class I R2 in the first shell coordination sphere of the metal center. In *Ct* R2 the metal center is coordinated by four glutamates, in contrast to three glutamates and one aspartate in *Escherichia coli* (*Ec*) R2. The aspartate is conserved in R2 proteins of other species and is a difference between RNR and other diiron carboxylate proteins, such as methane monooxygenase (MMO) which has four glutamates (*8*).

Biochemical studies of *Ct* R2 showed no evidence of a tyrosyl radical, consistent with the sequence studies and crystal structure (*9, 10*). The activity of *Ct* RNR was instead explained by an Fe(III)Fe(IV) state acting as the radical generating cofactor. This state has the same oxidation state as compound X in conventional class I R2 (*11, 12*), which has not yet been structurally determined. Compound X, formed directly after the oxygen cleavage at the diiron site, is responsible for generating the active state with the tyrosyl radical. ENDOR, EXAFS, Mössbauer, EPR, and MCD spectra have been interpreted to suggest different conformations, i.e., bis-μ-oxo-Fe(III)Fe(IV) (*13*) or μ-oxo-μ-hydroxo-Fe(III)Fe(IV) (*14*). If the radical generating cofactor in *Ct* R2 is a stable Fe(III)Fe(IV) state, this could indicate a role of compound X in conventional class I RNR in the catalytic reaction beyond generation of the tyrosyl radical. *Ct* R2 could also be a useful system for studying compound X.

* To whom correspondence should be addressed. Phone: +46 8 16 1268. Fax: +46 8 15 3679. E-mail: katarina.roos@physto.se.

[1] Abbreviations: *Ct*, *Chlamydia trachomatis*; *Ec*, *Escherichia coli*; RNR, ribonucleotide reductase; R2, RNR subunit II; MMO, methane monooxygenase; ENDOR, electron−nuclear double resonance; EXAFS, extended X-ray absorption fine structure; EPR, electron paramagnetic resonance; MCD, magnetic circular dichroism; N_3-ADP, 2′-azido-2′-deoxyadenosine 5′-diphosphate; DFT, density functional theory; B3LYP, Becke's three-parameter exchange-correlation potential; UB3LYP, unrestricted B3LYP; B3LYP*, B3LYP with an exact exchange parameter value of 15%; ECP, effective core potential; PDB, Protein Data Bank.

10.1021/bi801695d CCC: $40.75
Published on Web 02/16/2009

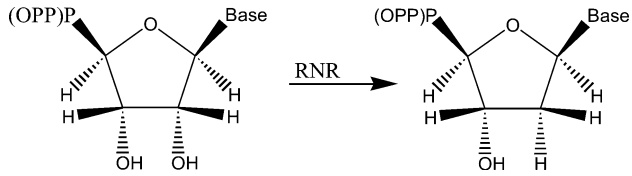

FIGURE 1: The substrate reaction catalyzed by RNR.

In 2007 Bollinger et al. showed, by enzyme activity measurements and spectroscopic methods, that the *Ct* R2 active radical generating cofactor instead has a mixed Mn(IV)Fe(III) metal center (*15*), later confirmed by Gräslund et al. (*16*) The activity observed earlier with an Fe(III)Fe(IV) cofactor was suggested to result from a Mn(IV)Fe(III) contaminant.

Bollinger et al. made several experiments to show that Mn(IV)Fe(III) is the *Ct* R2 active state. His_6-affinity-tagged forms of *Ct* R2 were studied and showed no correlation between catalytic activity and iron content. When adding 2 equiv of Fe(II) to metal-depleted R2, the activity was not detectably increased. In contrast, addition of both Fe(II) and Mn(II) activated the metal-depleted R2 with a factor 50. A Mn(II):Fe(II) ratio of unity gave maximal activation, and a total of 2 equiv of metals was enough to give 85% of maximal activity. In analogy with conventional class I RNR, *Ct* R2 with Mn(II)Fe(II) may react with molecular oxygen to form a radical generating active form. Indeed, in O_2-free solution no activity was shown, but when the RNR reaction solution to which the Mn(II)Fe(II)-R2 solution was added contained O_2, or when the metal center was exposed to O_2 prior to addition to the assay solution, activity was observed.

The active MnFe form showed no electron paramagnetic resonance (EPR) signal, but the Mössbauer parameters established that the reaction with O_2 converts the iron site to Fe(III). The Mössbauer spectra showed that the complex has a paramagnetic ground state with integer total spin. EPR spectra of the complex additionally reduced by dithionite indicated a MnFe cluster with $S_{total} = {}^1/_2$. The Mössbauer spectra of this reduced form showed that the iron site is still Fe(III), and hence only Mn is reduced. The reduced Mn site has to have an even number of electrons to give $S_{total} = {}^1/_2$ together with Fe(III), so the only reasonable possibility is Mn(III). The active state would thus be Mn(IV)Fe(III), with antiferromagnetic coupling between Mn $S = {}^3/_2$ and Fe $S = {}^5/_2$ (*17*).

Treatment with the substrate analogue 2′-azido-2′-deoxyadenosine 5′-diphosphate (N_3-ADP), known to irreversibly reduce the tyrosyl radical in conventional class I RNR, confirmed the conclusion that Mn(IV)Fe(III) is the active radical cofactor. As predicted, treatment of *Ct* RNR with N_3-ADP gave rise to an EPR signal indicating an irreversible conversion of the EPR-silent Mn(IV)Fe(III) to the EPR-active Mn(III)Fe(III). Substitution of the inactivator with the natural substrate did not give rise to the same signal. Moreover, treatment of the Fe(III)Fe(IV) complex with N_3-ADP did not accelerate the decay of this complex, meaning that the iron-substituted cluster was incompetent of radical initiation.

A possible reason for why the bacteria has developed this novel active site has been suggested by Högbom et al. to be as an adaption to the host's immune system (*6*). The stable tyrosyl radical appears to be a target for nitric oxide (NO) produced by the immune system. The independence of the radical in *Ct* RNR may make the pathogen more resistant to NO. The hypothesis has been evaluated by examining the reactivities of the MnFe cluster toward hydrogen peroxide (*18*). By sequence analysis, R2 proteins with a phenylalanine instead of the radical harboring tyrosine have been identified in ~30 other organisms (*19*). Some of these are pathogens, for example, *Mycobacterium bovis*, *Tropheryma whipplei*, and *Mycobacterium tuberculosis*. The class Ic RNR of pathogens could be a suitable drug target, especially since antibiotic resistance is an increasing public health problem.

In this work, density functional theory (DFT) is used to study the active center in *C. trachomatis* R2. Results are presented that suggest an explanation for why the enzyme needs the manganese at the metal center instead of a second iron. Calculated (H^+, e^-)-binding energies give a rationalization for the finding of Bollinger et al. that the iron-substituted enzyme is inactive (*15*).

COMPUTATIONAL METHODS

Quantum chemical calculations were performed using unrestricted density functional theory (DFT). All calculations were done using the B3LYP hybrid density functional (*20*−*24*). Geometries were fully optimized at the UB3LYP/LACVP level using Jaguar 5.5 (*25*). The LACVP basis set as implemented in Jaguar is a standard double ζ basis set with an effective core potential (ECP) on the metals (*26*). Accurate energies were calculated in the optimized structures using UB3LYP/cc-pVTZ(-f), a triple ζ basis set with polarization functions on all atoms but not including *f* functions (*27*−*29*). The metals were treated with a triple ζ basis set, LACV3P+, with diffuse functions. Electrostatic solvation effects from the surrounding protein were evaluated with a self-consistent reaction field method, using a Poisson−Boltzmann solver as implemented in Jaguar (*30, 31*). The dielectric constant was set equal to 4.0 in line with previous modelings of enzymes (*32*). The probe radius was chosen to be 1.40 Å, corresponding to the water molecule. Solvation effects were calculated from the optimized structures using Jaguar 7.0 (*33*) and LACVP*, a double ζ basis set with polarization functions on all atoms except hydrogen. Some structures were also optimized at the UB3LYP/LACVP* level to obtain accurate distances to compare with experiments.

Based on benchmark tests of the B3LYP functional, an accuracy of 3−5 kcal mol^{-1} can be expected for computed relative energies of transition metal containing systems (*34, 35*). There have been indications that the B3LYP* functional, which uses 15% Hartree−Fock exchange instead of 20% as in B3LYP, reproduces results for transition metals better (*36, 37*). Therefore, all energies discussed below have been evaluated also at a B3LYP* level of theory in order to make a comparison.

RESULTS AND DISCUSSION

In this section the calculated results will be presented and discussed. In the first part the structure of the metal center, e.g., the position of the manganese and the protonation state, will be discussed. In the second part (H^+, e^-)-binding energies will be presented, and conclusions on why the manganese is important in *Ct* R2 will be drawn. Ligand structure and possible roles of the glutamate instead of the aspartate will be discussed in the last part.

Models. A model of the active site in *Ct* R2 was constructed based on the X-ray crystal structure (PDB code

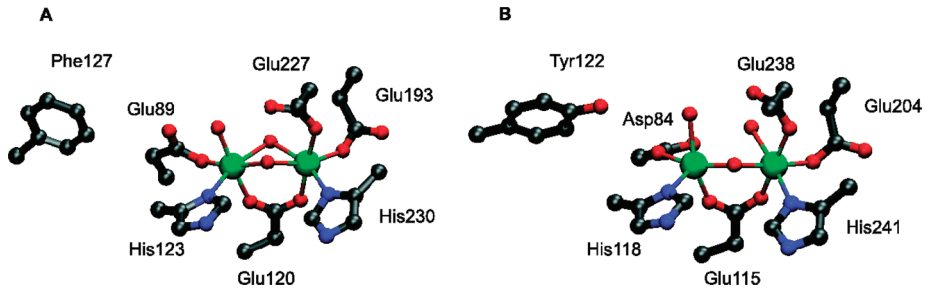

FIGURE 2: X-ray active site structures for *Ct* R2 (A) and *Ec* R2 met (*7*) (B). *Ct* R2 has a phenylalanine at the position of the tyrosine in *Ec* R2. The first shell ligand structure involves four glutamates in *Ct* R2 in contrast to three glutamates and one aspartate in *Ec* R2. Glu89 is in an up position in *Ct* R2, hydrogen bonding to the terminal water of the closest metal. The corresponding Asp84 in *Ec* R2 is in a down conformation, hydrogen bonding to the terminal water on the opposite metal.

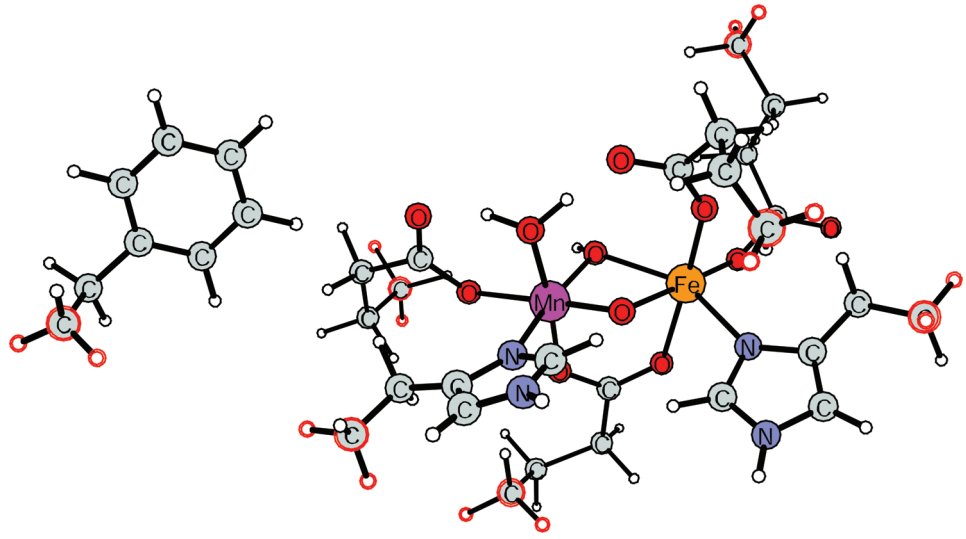

FIGURE 3: A model of the active site made from coordinates from the crystal structure. One of the iron centers in the crystal structure is replaced by manganese. Atoms marked with red are frozen in the calculations.

1SYY) (*6*) (Figure 3). The structure probably contains two irons in the diferric state. In order to compare with conventional class I R2, corresponding studies were made on a model based on the X-ray structure of the *Ec* R2 in its met (oxidized) state (PDB code 1MXR) (*7*). The metals, first shell ligands, and phenylalanine/tyrosine were included in the model. To reproduce the protein strain and positioning of the amino acids included, three coordinates are frozen on each amino acid, the α-carbon and two hydrogen atoms along the backbone. Calculations were made on the iron-substituted *Ct* R2, the *Ct* F127Y variant, and the *Ec* Y122F variant R2, the *Ct* E89D variant, and the *Ec* D84E variant R2, as well as on the native structures.

Metal Center. The available *Ct* R2 crystal structure is in the diferric state (*6*). In order to study the active center, a model of the active Mn(IV)Fe(III) state must be constructed. The structures discussed below are similar to the structures proposed for compound X in *Ec* R2 (*13, 14*). They have a diamond core structure with two O(H) bridges and one terminal water or hydroxide.

The first question to be answered is in which metal site the manganese is positioned. Calculations show that the neutral μ-oxo-μ-hydroxo structure with the manganese in the position closest to the phenylalanine (position 1) is 1.2 kcal mol^{-1} lower in energy than the corresponding one with manganese in the other metal site (Figure 4). The same is true for the negatively charged bis-μ-oxo structure (model without phenylalanine, 1.1 kcal mol^{-1}). The small energy difference makes the assignment of position 1 for Mn rather uncertain. From arguments about the proximity of position 1 to the electron transfer chain and the observed change exclusively of the oxidation state of MnIV in the activated state, Mn in position 1 is consistent with experiments, as concluded by Roth et al. (*38*) However, for a complete picture, some of the calculations below were also made on a model with Mn in position 2. The difference in energetics between having a higher oxidation state on Fe instead of Mn is larger, 14.4 kcal mol^{-1}, showing that Mn(IV)Fe(III) is much more stable than Mn(III)Fe(IV), consistent with experiments (*15, 17*). In *Ec* R2 with two irons the μ-oxo-μ-hydroxo structure with Fe(IV) in position 1 is 0.6 kcal mol^{-1} lower in energy than with Fe(IV) in position 2. However, the energy difference calculated here is too small to draw any firm conclusions. Experimental work has suggested that the ferryl iron is instead in position 2 in compound X (*39*−*41*). Since the energy difference is so small, the conclusions drawn below are not affected by the position of Fe(IV).

Another important question concerning the structure of the metal center is the protonation state of the bridge. The *Ct* R2 bis-μ-oxo-Mn(IV)Fe(III) and μ-oxo-μ-hydroxo-Mn(IV)Fe(III) structures with terminal water bound to the metal in position 1 and a bridging carboxylate are therefore compared. A hydroxo bridge by oxygen b (O^b in Figure 4), on the opposite side to the histidine ligands, is 8.7 kcal mol^{-1} more favorable than a hydroxo bridge by O^a (calculated for

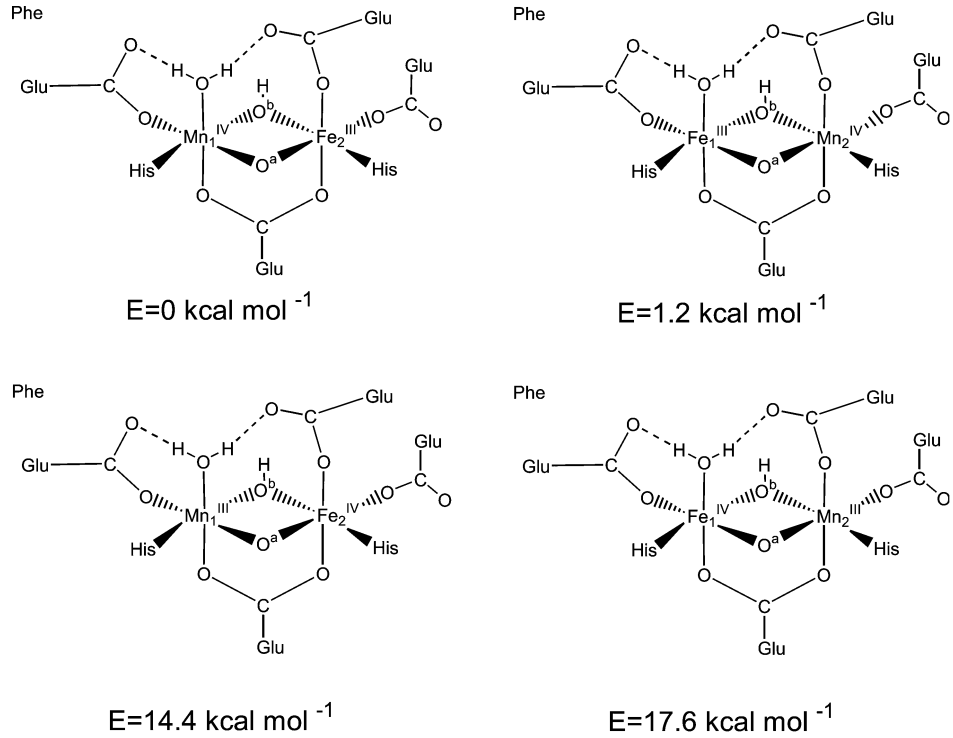

FIGURE 4: Metal center in *Ct* R2. The most energetically favorable active state has Mn(IV) in position 1.

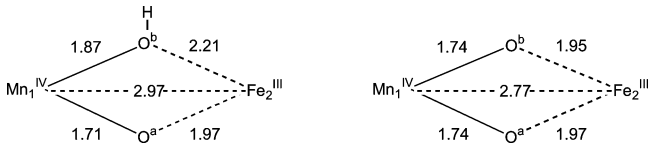

FIGURE 5: Calculated distances, in Å, for the bis-μ-oxo-bridged and μ-oxo-μ-hydroxo-bridged structures in the active Mn(IV)Fe(III) state.

a model without the phenylalanine). Calculated distances in the two structures are compared to EXAFS measurements of a Mn(IV)−Fe(III) distance of 2.75 Å and shortest Mn−O distance of 1.65 Å (*42*) (Figure 5). The calculated metal−metal distances are 2.97 Å for the μ-oxo-μ-hydroxo-Mn(IV)Fe(III) structure and 2.77 Å for the bis-μ-oxo-Mn(IV)Fe(III) structure. The shortest calculated Mn−O distances are 1.71 and 1.74 Å for the μ-oxo-μ-hydroxo-Mn(IV)Fe(III) and bis-μ-oxo-Mn(IV)Fe(III), respectively. The same trend with a shorter metal(IV)−O_{oxo} distance in the μ-oxo-μ-hydroxo structure has been observed for compound X, where Mitic et al. calculated the Fe(IV)−O_{oxo} distances to 1.70 Å for the μ-oxo-μ-hydroxo-Fe(III)Fe(IV) structure and 1.73 Å for the bis-μ-oxo-Fe(III)Fe(IV) structure (*14*). B3LYP with the present basis sets is known to overestimate metal−metal distances in this type of systems (*43*). With this in mind, the structure in best agreement with the experiments is the μ-oxo-μ-hydroxo-Mn(IV)Fe(III). In an EXAFS and computational study published at the stage of revision, Bollinger et al. also preferred a μ-oxo-μ-hydroxo structure (*44*). In addition, optimization of the minus one charged system shows that the μ-oxo-μ-hydroxo-Mn(IV)Fe(III) with a terminal hydroxide is energetically lower, 3.5 kcal mol^{-1}, than the bis-μ-oxo-Mn(IV)Fe(III) with a terminal water. This is an additional argument why the active state structure should have a hydroxo bridge.

Proton affinities were calculated for the *Ct* R2 active state and *Ec* R2 met (oxidized) state, shown in Table 1. Note that relative proton affinities are reasonable, while absolute values lack meaning in the protein environment. The *Ec* R2 met state is known to have a μ-oxo-Fe(III)Fe(III)-$(H_2O)_2$-structure; i.e., the hydroxo bridge is protonated, forming a terminal water (*7, 45*). The proton affinity of adding a proton to the terminal hydroxide of the negatively charged *Ct* R2 Mn(IV)Fe(III) state is only 0.4 kcal mol^{-1} lower than that of adding a proton to the hydroxo bridge of the negatively charged *Ec* R2 met state. The pK_a value for the bridging water in the *Ec* R2 met state is thus the same as for the terminal water in the *Ct* R2 active state. Since the bridging group in the *Ec* R2 met state is a water, the terminal group in the *Ct* R2 active state should also be a water, forming a neutral active state structure with one μ-oxo bridge, one μ-hydroxo bridge, and one terminal water.

Table 1: Proton Affinities of the *Ct* R2 Active State and *Ec* R2 Met State[a]

		proton affinities (kcal mol^{-1})
Ec met state	[μ-oxo-μ-hydroxo-Fe(III)Fe(III)-H_2O/Tyr]$^-$ + H^+ → [μ-oxo-Fe(III)Fe(III)-$(H_2O)_2$/Tyr]^0	306.0
Ct active state	[μ-oxo-μ-hydroxo-Mn(IV)Fe(III)-OH/Phe]$^-$ + H^+ → [μ-oxo-μ-hydroxo-Mn(IV)Fe(III)-H_2O/Phe]^0	305.6

[a] Note that only relative proton affinities should be used. *Ec* R2 met is known to have two terminal waters.

Based on the discussion above, the *Ct* R2 active state structure that was most extensively studied in this work is the μ-oxo-μ-hydroxo-Mn(IV)Fe(III)-H_2O; however, calculations were also made for the μ-oxo-μ-hydroxo-Mn(IV)Fe(III)-OH structure.

(H^+, e^-)-Binding Energies. When the radical is transferred from subunit R2 to R1, there are two possibilities for the radical initiating step. Either an electron and a proton are added to the R2 active state structure or only an electron is added. On the basis of previous studies the proton is assumed

to be taken initially from the bulk and the electron from Trp48 (*46*). The second case when only the electron enters the active site from outside will be discussed in a later paragraph. In the first case, the proton and electron are added to the tyrosyl radical in *Ec* R2. The product should be similar to the met state crystal structure, which suggests a mono-μ-oxo-bridged Fe(III)Fe(III) structure with a terminal water on Fe2, one on Fe1, and neutral Tyr122 (*7*). The active state was assumed to have the same structure as the met state but with a tyrosyl radical. In *Ct* R2 the proton and electron are added to the Mn(IV)Fe(III) metal center forming a Mn(III)Fe(III) state. The crystallographically observed *Ct* R2 state was initially suggested to have a bis-μ-hydroxo-bridged Fe(III)Fe(III) structure (*6*). With Mn instead of one of the irons, the calculations indicate that the corresponding Mn(III)Fe(III) state with a bis-μ-hydroxo-bridged structure and one terminal water is energetically 2.6 kcal mol^{-1} more unstable than with a mono-μ-oxo-bridged structure and two terminal waters. Again, the accuracy of the calculation is hardly enough for a firm prediction.

As mentioned in the introduction, the difference in proton-coupled redox potential between the active state in R2 and the cysteine in R1 is crucial for activity. This difference must be carefully tuned to allow for the radical transfer to be reversible. The assumption is that the redox potential of the catalytically active cysteine in R1 is the same in *Ct* as in *Ec*. The redox potential of the R2 active states should then also be the same. In *Ec* R2 the radical generating cofactor is the tyrosine radical, Tyr122(rad), whereas in *Ct* R2 it is the Mn(IV)Fe(III) metal center. (H^+, e^-)-binding energies for the radical generating cofactors in *Ec*, native *Ct*, and iron-substituted *Ct* R2 were compared. (H^+, e^-)-binding energies are calculated by taking the difference in energy of the complex when adding a proton and an electron minus the energy of a hydrogen atom in gas phase. The (H^+, e^-)-binding energies should differ from the proton-coupled redox potentials mainly by a constant. For example, if the calculated (H^+, e^-)-binding energies are the same for two systems, their redox potentials should also be the same. The calculated (H^+, e^-)-binding energy is 92.8 kcal mol^{-1} for the active *Ct* R2 Mn(IV)Fe(III) state, where the proton binds to the hydroxo bridge of the metal center and the electron reduces Mn(IV) to Mn(III) (Figure 6). Indeed, the corresponding (H^+, e^-)-binding energy for the *Ec* R2 active form, where the hydrogen atom is added to the tyrosyl radical, is 91.4 kcal mol^{-1}, a very similar value. The calculated redox potential difference between *Ct* R2 Mn(IV)Fe(III) and the *Ec* R2 tyrosyl radical is thus 0.06 V. The difference is almost the same if Mn is in position 2. The (H^+, e^-)-binding energy is then 94.0 kcal mol^{-1}. The corresponding (H^+, e^-)-binding energy for the iron-substituted *Ct* R2 active state is higher, 105.0 kcal mol^{-1}. Hence, the Fe(III)Fe(IV) metal center has a higher calculated redox potential by 0.53 V and is therefore a substantially stronger oxidant than the Mn(IV)Fe(III) metal center.

Also, (H^+, e^-)-binding energies for the minus one charged μ-oxo-μ-hydroxo systems with a terminal hydroxide were calculated (Figure 6). The proton is added to the terminal hydroxide, forming terminal water, and the electron reduces Mn(IV) or Fe(IV). The (H^+, e^-)-binding energies are 92.1 and 103.9 kcal mol^{-1} for the active state in *Ct* and iron-substituted *Ct* R2, respectively. The difference between the

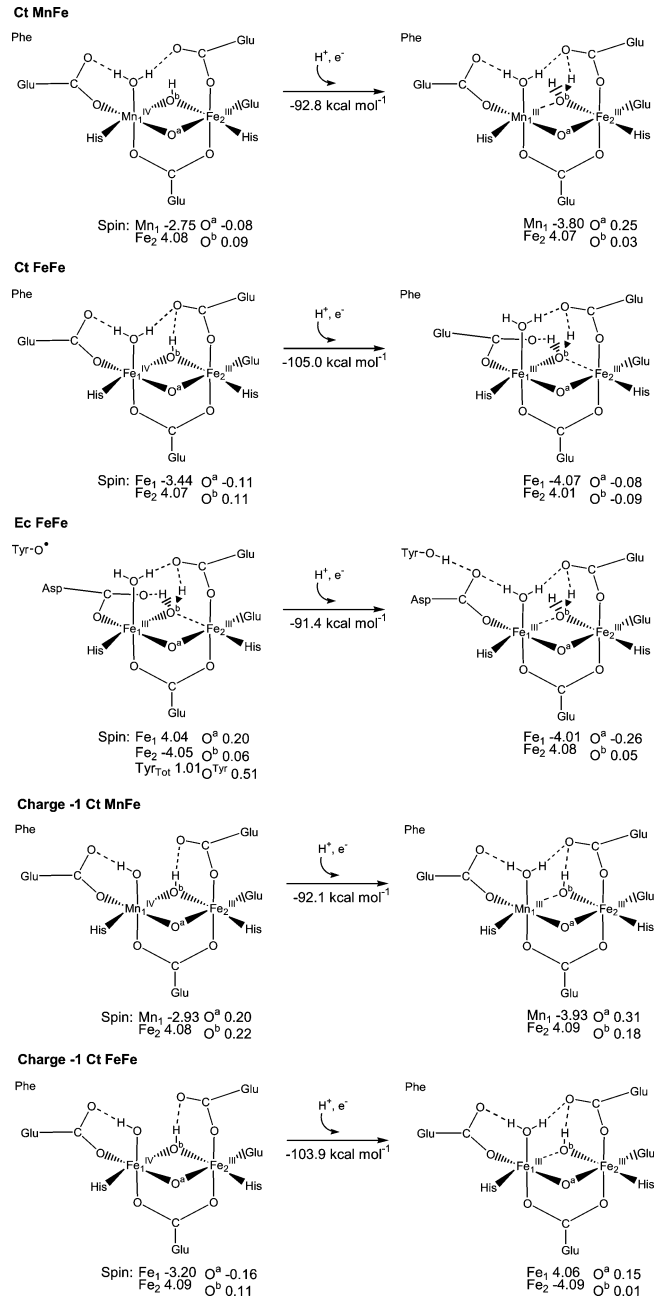

FIGURE 6: (H^+, e^-)-binding energies for the radical generating states in *Ct*, iron-substituted *Ct*, and *Ec* R2.

binding energies of *Ct* and iron-substituted *Ct* R2 is 11.8 kcal mol^{-1} compared to 12.2 kcal mol^{-1} for the protonated system. The difference between the (H^+, e^-)-binding energies of the negatively charged *Ct* R2 active state and the *Ec* R2 active state is 0.7 kcal mol^{-1} compared to 1.4 kcal mol^{-1} for the neutral *Ct* R2 active state. Hence, the same conclusions can be drawn as for the protonated systems.

To further compare the oxidative strength of Mn(IV) and Tyr(rad), the *Ct* F127Y variant R2 was studied. The energy differences between the active Tyr(rad) state and a preceding Fe(III)Fe(IV) state, and corresponding Mn(IV)Fe(III) state in *Ct* F127Y R2, were calculated. In *Ec* R2 the hydrogen atom transfer from Tyr122 to the metal center to produce the active state with Tyr122(rad) is exothermic with 13.3 kcal mol^{-1} (0.58 V) (Figure 7). In *Ct* F127Y R2 with Mn(IV)Fe(III) the corresponding transfer is almost isothermic with an endothermicity of only 0.2 kcal mol^{-1} (0.01 V).

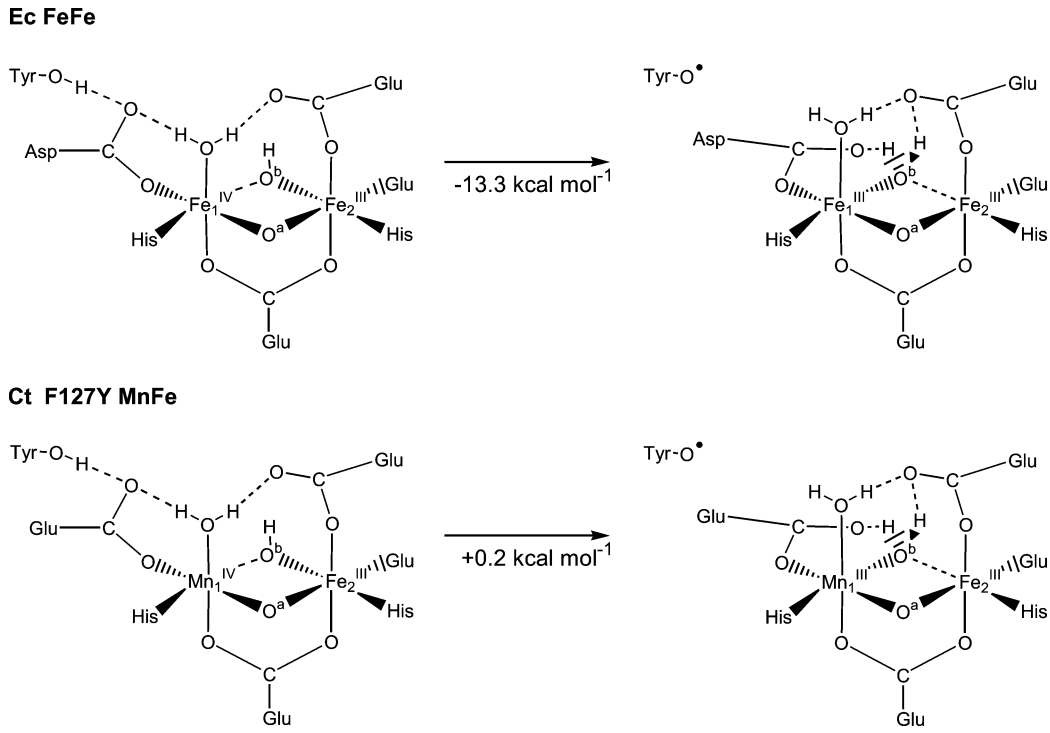

FIGURE 7: Comparison of oxidative strength of Mn(IV) and Tyr(rad). Energy difference between the active Tyr(rad) state and a preceding Fe(III)Fe(IV) state and corresponding in *Ct* F127Y R2.

Hence, in *Ct* F127Y R2, Mn(IV) is an equally strong oxidant as a tyrosyl radical in the place of Phe127.

The conclusion that can be drawn from the calculated results above is that Mn is needed to lower the proton-coupled redox potential. In *Ec* R2, the proton-coupled electron transfer from Tyr122 to the metal center of compound X to produce the active state with Tyr122(rad) reduces the proton-coupled redox potential with 0.58 V. In the absence of Tyr a less strong oxidant than Fe(III)Fe(IV) is needed. *Ct* R2 is active with Mn at the metal center, and the proton-coupled redox potential of the iron-substituted Fe(III)Fe(IV) center is 0.53 V higher for the neutral system. The conclusion can be drawn that the iron-substituted *Ct* R2 would have a too strong proton-coupled redox potential and most probably therefore not be active. The Fe(III)Fe(IV) metal center is such a strong oxidant that it would probably abstract an electron from the surrounding, leading to a shortcut and an inactivation of the enzyme. In principle, the results cannot exclude that Fe(III)Fe(IV) is potent of driving one single reaction cycle, since Fe(III)Fe(IV) is potent of driving the radical transfer from R2 to R1. However, the transfer in the reverse direction should not be possible since the metal center has a too high redox potential compared to the one of the catalytic cysteine in R1. Therefore, no second substrate reaction cycle should be possible. In addition, Bollinger et al. have showed that the iron-substituted complex is not even active one cycle with the substrate analogue N_3-ADP (*15*). Hence, because of their different redox potentials it is not possible to substitute Mn with Fe in *Ct* RNR.

The same conclusions are also valid for the redox potentials, when only an outside electron is added to the active state but no outside proton. In *Ec* R2 the proton could be taken from the terminal water on Fe1 and transferred to Tyr122. The complex is thereafter rearranged to the lowest state with terminal water and a hydroxo bridge. In *Ct* R2 the calculated (e^-)-binding energy is the difference between the energy of the neutral μ-oxo-μ-hydroxo-Mn(IV)Fe(III)-H_2O and the one electron reduced μ-oxo-μ-hydroxo-Mn(III)Fe(III)-H_2O. In *Ec* R2 the calculated (e^-)-binding energy is the difference between the energy of the μ-oxo-Fe(III)Fe(III)-$(H_2O)_2$/Tyr(rad) and the μ-oxo-μ-hydroxo-Fe(III)Fe(III)-H_2O/Tyr. The (e^-)-binding energies are 101.5, 100.5, and 111.5 kcal mol^{-1} for the active state in *Ct*, *Ec*, and iron-substituted *Ct* R2, respectively. The difference between the binding energies of the active state of *Ct* and *Ec* R2 is now 1.0 kcal mol^{-1} compared to 1.4 kcal mol^{-1} for the (H^+, e^-)-binding energies of the neutral system above. The difference between *Ct* and iron-substituted *Ct* R2 is 10.0 kcal mol^{-1} compared to 12.2 kcal mol^{-1}.

The active state metal complex in R2 is probably a neutral μ-oxo-μ-hydroxo-Mn(IV)Fe(III) with terminal water. Calculations show that Mn(IV) is an equally strong oxidant as the Tyr122(rad) in *Ec* R2 and that Fe(IV) is a too strong oxidant. However, even if the system is negatively charged, the same conclusions are valid. The most relevant property is the proton-coupled redox potential, which is related to the (H^+, e^-)-binding energy. However, the same qualitative conclusions can be drawn from the (e^-)-binding energies.

15% Hartree−Fock Exchange. The binding energies discussed above were also evaluated using the B3LYP* functional. The results are consistent with the above results and experiments. The difference between the (H^+, e^-)-binding energy for the *Ec* R2 and neutral *Ct* R2 is −3.3 kcal mol^{-1} with B3LYP* compared to 1.4 kcal mol^{-1} with B3LYP. The corresponding difference between iron-substituted *Ct* R2 and *Ec* R2 is 8.9 kcal mol^{-1} with B3LYP* compared to 13.6 kcal mol^{-1} with B3LYP. The difference between the (H^+, e^-)-binding energy of *Ct* and iron-substituted *Ct* R2 is still as large, 12.2 kcal mol^{-1} both with B3LYP* and B3LYP. So, knowing from experiments that

Table 2: Energy Differences between the Two Conformations of Glu89/Asp84 in the Product Metal(III)Metal(III) Structure for Different Variants[a]

species	metals	amino acid 89/84	amino acid 127/122	*E* down rel up (kcal mol^{-1})
Product Metal(III)Metal(III) State				
Ct	MnFe	Glu	Phe	+0.6
Ct	FeFe	Glu	Phe	−1.1
Ct F127Y	MnFe	Glu	Tyr	+8.8
Ct F127Y	FeFe	Glu	Tyr	+8.2
Ct E89D	MnFe	Asp	Phe	+0.6
Ct E89D	FeFe	Asp	Phe	−1.6
Ec	FeFe	Asp	Tyr	+0.7
Ec	MnFe	Asp	Tyr	+3.3
Ec Y122F	FeFe	Asp	Phe	+1.5
Ec Y122F	MnFe	Asp	Phe	+3.3
Ec D84E	FeFe	Glu	Tyr	+8.3
Active State with Tyr(rad)				
Ec	FeFe	Asp	Tyr	−2.4
Ec D84E	FeFe	Glu	Tyr	−0.1

[a] The flexibility of Glu89/Asp84 may be involved in proton transfer.

the enzyme is active with Mn, the conclusion why it will not be active with Fe is still valid for B3LYP* with the same certainty.

Glutamate versus Aspartate. As mentioned in the introduction, the active site of *Ct* R2 has a different ligand structure than the one of *Ec* R2. Asp84 that is conserved in RNR from different species is in *Ct* R2 replaced by Glu89. This motif with four coordinating glutamates is the same as in MMO. In order to try to explain the role of this fourth glutamate in *Ct* R2, the two different positions of the Glu/Asp in the product metal(III)metal(III) state, the up position as in the *Ct* R2 structure and the down position as in the *Ec* R2 structure (Figure 2), were studied for different *Ct* and *Ec* R2 variants. In all variational studies the α-carbon and two hydrogen atoms along the backbone are frozen as for the native amino acid. To change Asp84 to Glu in *Ec* R2 for example, a CH_2 link is added between the α- and β-carbon. The assumption is thus that the backbone position is not affected by the variation. In nature the α-carbons have some flexibility, not accounted for in the calculations. This may affect the conclusions somewhat. Asp84 in *Ec* RNR has been suggested to be involved in proton-coupled electron transfer between Tyr122 and the diiron complex (*46*). The flexibility of Asp84 is thus important, and the energy for the reactant up and product down position should ideally be similar. Indeed, the calculated energy differences between the up and down position are within a couple of kilocalories per mole for most structures studied (Table 2). In particular, note that the *Ct* E89D variant R2 has exactly the same energy difference between the up and down conformation as the native *Ct* R2 structure. This indicates that the enzyme could work as well with Asp89, at least in terms of this aspect, and shows no different role of Glu than Asp for this particular transfer.

The only exceptions are the *Ct* F127Y variant, the iron-substituted *Ct* F127Y variant, and the *Ec* D84E variant R2. The energy differences between the up and down structure for these compounds are all around 8 kcal mol^{-1}. In particular, the energy difference for the *Ec* D84E variant R2 is 8.3 kcal mol^{-1}. According to the results, in the presence of Tyr there is a difference in strain between having Glu or Asp at this position in the active center, due to the additional carbon link in Glu. The hydrogen bond from Tyr122 to the carboxylate group of Glu84 in the down position in *Ec* D84E R2 is 0.10Å longer than the corresponding from Tyr122 to Asp84 in *Ec* R2 (Figure 8). This stretch does not give a large energy difference by itself but indicates a difference in strain. The Fe1 site in the *Ec* D84E R2 up structure has an octahedral coordination. Fe1 in the corresponding native *Ec* R2 structure has a nonoctahedral coordination with an angle of 142° between Wat1−Fe1−Glu115, and Wat2 is bound to Fe2. Asp is shorter than Glu and may not be able to reach in between Tyr122 and Wat1 to form the octahedral structure, possibly destabilizing the up structure and thereby decreasing the energy difference between the up and down structure. It should be noted that the distances in the structures only show minor effects of a switch between Asp and Glu, and energy calculations are therefore essential. The crystal structure of the diferric *Ec* D84E R2 (PDB code 1PIU) has Glu84 in an up position (*47*), as the *Ct* R2 crystal structure (*6*), and in contrast to the *Ec* R2 met structure (*7*). The finding that the down position is energetically less stable than the up position for the *Ec* D84E R2 variant is hence in agreement with the crystal structure. The large energy differences between the up and down conformations of all variants with Glu and Tyr indicate that this is a nonoptimal combination that decreases the flexibility of the amino acid. This may be a reason why *Ec* RNR contains an Asp instead of the Glu that is conserved in MMO. *Ct* RNR lacks the tyrosine, and therefore a switch to aspartate is not necessary. Assuming that *Ct* RNR evolved from *Ec* RNR evolutionarily, this cannot explain why there is a fourth glutamate in *Ct* R2. However, the results may give an indication to why *Ec* R2 has an aspartate in contrast to other diiron carboxylate proteins. If on the other hand *Ct* RNR evolved before or simultaneously to *Ec* RNR from a common MMO-like ancestor, the results above may explain why Glu was exchanged for Asp in *Ec* R2 but not in *Ct* R2. To further investigate the role of Glu89 in *Ct* R2 and Asp84 in *Ec* R2, calculations should be made also on the oxygen cleaving reaction of both enzymes and all relevant variants.

Another possible role for Glu89 in *Ct* R2 is to increase the binding energy of Mn at the active site. Calculations were made on the product Mn(III)Fe(III) state. The energy differences between the *Ct* R2 product structures with Mn and with Fe were calculated. These differences were then compared to the corresponding ones for the *Ct* E89D R2 product structures. The calculations showed no difference in binding energy of Mn relative to Fe depending on Glu or Asp. However, the metals bind in the +II oxidation state, and the same calculations should be made for the reduced Mn(II)Fe(II) state before oxygen binding.

Jahn−Teller Axis for Mn(III). In the product Mn(III)Fe(III) state of *Ct* R2, Glu89 is in an up position, according to the crystal structure. However, a structure resembling the *Ec* R2 met structure, with Glu89 in a down position, has the same energy (0.6 kcal mol^{-1} energy difference, Table 2). Because of the similarity to the *Ec* R2 met state, the structure with Glu89 in the down position may be important. The position of Wat2 in the two structures can be explained by their different Jahn−Teller axes (Figure 9). Mn(III) with high spin has four unpaired d-electrons. With an octahedral conforma-

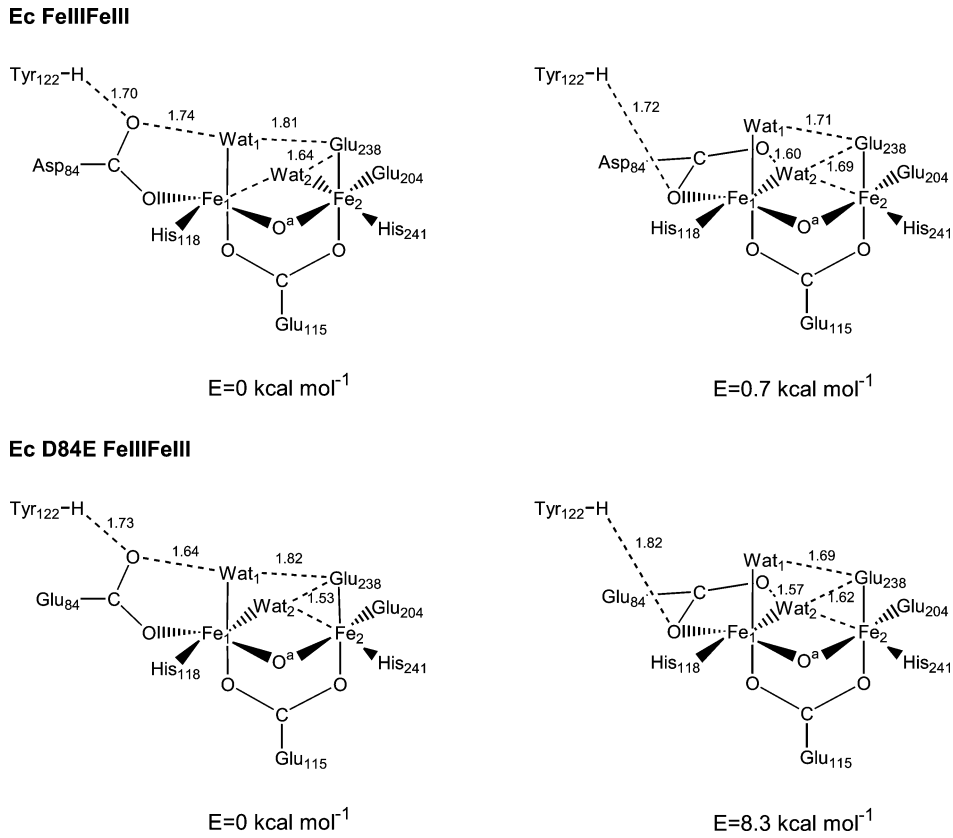

FIGURE 8: Structures and energy differences for the met structures with Asp84 in its up or down position for *Ec* native and D84E variant R2. All distances are in Å.

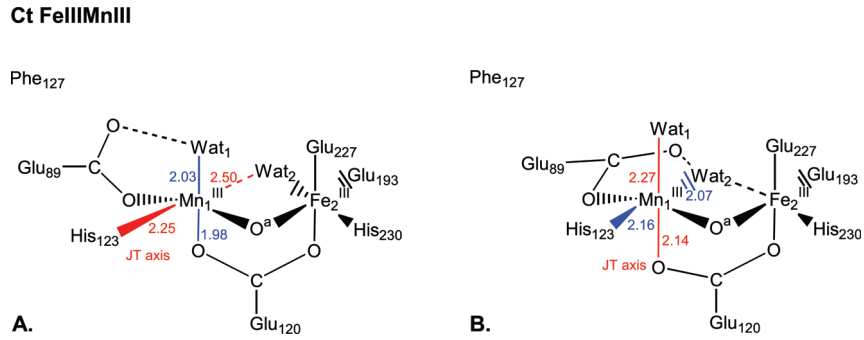

FIGURE 9: Jahn−Teller axis, marked in red, for the *Ct* R2 product Mn(III)Fe(III) state with Glu89 in the up position (A) and with Glu89 in the down position (B). All distances are in Å.

tion as in R2 there are degenerate states, which distort and gain energy by the Jahn−Teller effect, and Mn(III) has a profound Jahn−Teller axis. When Glu89 is in an up position, it accepts a hydrogen bond from the terminal water on the manganese (Wat1 in Figure 9A). The water gets a slightly negative hydroxo group character, making the bond to the metal strong and therefore short, 2.03 Å. The Jahn−Teller axis is therefore along the second water (Wat2), the metal, and His123. The Mn−Wat2 distance is 2.50 Å, and the Mn−His123 bond is long, 2.25 Å. In the up structure the two waters are therefore coordinated to opposite metals. If Glu89 is flipped down to accept a hydrogen bond from Wat2, the situation is changed (Figure 9B). Wat2 now gets a negative hydroxo group character, and the bond to Mn is short and strong, 2.07 Å. The Jahn−Teller axis is now instead the Wat1−Mn−Glu120 axis. The Wat1−Mn bond is 2.27 Å, and the distance between Mn and the coordinating oxygen of Glu120 is 2.14 Å compared to 1.98 Å for the up conformation. In the down conformation both terminal waters are thus coordinated to the same metal.

CONCLUSIONS

Experimental groups have shown that *C. trachomatis* R2 lacks the tyrosine crucial for activity in conventional RNR and instead has Mn(IV) at the active center. The main purpose of the present study is to explain why this novel form of R2 needs manganese and why it would not also work with iron. DFT calculations show that Mn is needed because of its lower redox potential. Fe(IV) has a too high redox potential and would therefore generate an inactive *Ct* R2 protein. The Mn(IV)Fe(III) active center is an equally strong oxidant as the active state in *E. coli* R2 with a tyrosyl radical. When forming the active state in *Ec* R2 from a preceding

compound X with oxidation state Fe(III)Fe(IV), the redox potential of the active center is lowered. In the absence of the tyrosine, a less strong oxidant is needed. The calculations also show that Mn(IV) is equally strong as a tyrosyl radical in the *Ct* F127Y variant R2, further supporting the conclusion.

In addition to the absence of the normally conserved radical harboring Tyr and the presence of Mn in the active center, *Ct* R2 also has a slightly different first shell ligand structure with Glu89 instead of Asp84 in *Ec* R2. Calculations show a difference in flexibility of Glu and Asp in the presence of Tyr. The results indicate that Glu is less flexible than Asp in combination with Tyr. In *Ec* R2, Asp84 is assumed to be involved in proton-coupled electron transfer. The flexibility of the amino acid is therefore important. A difference between Glu and Asp may thus explain why there is an aspartate in *Ec* R2, in contrast to, e.g., MMO. *Ct* R2 and *Ec* R2 may have evolved simultaneously from a common ancestor. Since *Ct* R2 lacks the tyrosine, an aspartate is not necessary for good flexibility, but glutamate works as well. In *Ec* R2, on the other hand, the presence of Tyr122 makes the flexibility of a glutamate at this position poor, and an ancestral bacterium with a mutant R2 with Asp84 could have gained a selective advantage.

The calculations on *Ct* R2 performed in this study have shed some light on the properties and function of this novel active site but have also given insight into some questions still not solved for *Ec* R2.

REFERENCES

1. Nordlund, N., and Reichard, P. (2006) Ribonucleotide reductases. *Annu. Rev. Biochem. 75*, 681–706.
2. Nordlund, P., Sjöberg, B.-M., and Eklund, H. (1990) Three-dimensional structure of the free radical protein of ribonucleotide reductase. *Nature 345*, 593–598.
3. Reece, S. Y., Hodgkiss, J. M., Stubbe, J., and Nocera, D. G. (2006) Proton-coupled electron transfer: the mechanistic underpinning for radical transport and catalysis in biology. *Philos. Trans. R. Soc. London, Ser. B 361*, 1351–1364.
4. Siegbahn, P. E. M., Eriksson, L., Himo, F., and Pavlov, M. (1998) Hydrogen atom transfer in ribonucleotide reductase (RNR). *J. Phys. Chem. B 102*, 10622–10629.
5. Roshick, C., Iliffe-Lee, E. R., and McClarty, G. (2000) Cloning and characterization of ribonucleotide reductase from *Chlamydia trachomatis*. *J. Biol. Chem. 275*, 38111–38119.
6. Högbom, M., Stenmark, P., Voevodskaya, N., McClarty, G., Gräslund, A., and Nordlund, P. (2004) The radical site in chlamydial ribonucleotide reductase defines a new R2 subclass. *Science 305*, 245–248.
7. Högbom, M., Galander, M., Andersson, M., Kolberg, M., Hofbauer, W., Lassmann, G., Nordlund, P., and Lendzian, F. (2003) Displacement of the tyrosyl radical cofactor in ribonucleotide reductase obtained by single-crystal high-field EPR and 1.4-ångstrom x-ray data. *Proc. Natl. Acad. Sci. U.S.A. 100*, 3209–3214.
8. Merkx, M., Kopp, D. A., Sazinsky, M. H., Blazyk, J. L., Muller, J., and Lippard, S. J. (2001) Dioxygen activation and methane hydroxylation by soluble methane monooxygenase: A tale of two irons and three proteins. *Angew. Chem., Int. Ed. 40*, 2782–2807.
9. Voevodskaya, N., Lendzian, F., and Gräslund, A. (2005) A stable Fe-III-Fe-IV replacement of tyrosyl radical in a class I ribonucleotide reductase. *Biochem. Biophys. Res. Commun. 330*, 1213–1216.
10. Voevodskaya, N., Narvaez, A. J., Domkin, V., Torrents, E., Thelander, L., and Gräslund, A. (2006) Chlamydial ribonucleotide reductase: Tyrosyl radical function in catalysis replaced by the Fe-III-Fe-IV cluster. *Proc. Natl. Acad. Sci. U.S.A. 103*, 9850–9854.
11. Bollinger, J. M., Edmondson, D. E., Huynh, B. H., Filley, J., Norton, J. R., and Stubbe, J. (1991) Mechanism of assembly of the tyrosyl radical-dinuclear iron cluster cofactor of ribonucleotide reductase. *Science 253*, 292–298.
12. Sturgeon, B. E., Burdi, D., Chen, S. X., Huynh, B. H., Edmondson, D. E., Stubbe, J., and Hoffman, B. M. (1996) Reconsideration of X, the diiron intermediate formed during cofactor assembly in *E. coli* ribonucleotide reductase. *J. Am. Chem. Soc. 118*, 7551–7557.
13. Han, W. G., Liu, T. Q., Lovell, T., and Noodleman, L. (2006) Seven clues to the origin and structure of class-I ribonucleotide reductase intermediate X. *J. Inorg. Biochem. 100*, 771–779.
14. Mitic, N., Clay, M. D., Saleh, L., Bollinger, J. M., and Solomon, E. I. (2007) Spectroscopic and electronic structure studies of intermediate X in ribonucleotide reductase R2 and two variants: A description of the Fe-IV-oxo bond in the Fe-III-O-Fe-IV dimer. *J. Am. Chem. Soc. 129*, 9049–9065.
15. Jiang, W., Yun, D., Saleh, L., Barr, E. W., Xing, G., Hoffart, L. M., Maslak, M. A., Krebs, C., and Bollinger, J. M. (2007) A manganese(IV)/iron(III) cofactor in *Chlamydia trachomatis* ribonucleotide reductase. *Science 316*, 1188–1191.
16. Voevodskaya, N., Lendzian, F., Ehrenberg, A., and Gräslund, A. (2007) High catalytic activity achieved with a mixed manganese-iron site in protein R2 of *Chlamydia* ribonucleotide reductase. *FEBS Lett. 581*, 3351–3355.
17. Jiang, W., Bollinger, J. M., and Krebs, C. (2007) The active form of *Chlamydia trachomatis* ribonucleotide reductase R2 protein contains a heterodinuclear Mn(IV)/Fe(III) cluster with $S = 1$ ground state. *J. Am. Chem. Soc. 129*, 7504–7505.
18. Jiang, W., Xie, J. J., Norgaard, H., Bollinger, J. M., and Krebs, C. (2008) Rapid and quantitative activation of *Chlamydia trachomatis* ribonucleotide reductase by hydrogen peroxide. *Biochemistry 47*, 4477–4483.
19. Jiang, W., Saleh, L., Barr, E. W., Xie, J. J., Gardner, M. M., Krebs, C., and Bollinger, J. M. (2008) Branched activation- and catalysis-specific pathways for electron relay to the manganese/iron cofactor in ribonucleotide reductase from *Chlamydia trachomatis*. *Biochemistry 47*, 8477–8484.
20. Becke, A. D. (1988) Density-functional exchange-energy approximation with correct asymptotic behavior. *Phys. Rev. A 38*, 3098–3100.
21. Becke, A. D. (1993) A new mixing of Hartree-Fock and local density-functional theories. *J. Chem. Phys. 98*, 1372–1377.
22. Becke, A. D. (1993) Density-functional thermochemistry. III. The role of exact exchange. *J. Chem. Phys. 98*, 5648–5652.
23. Lee, C. T., Yang, W. T., and Parr, R. G. (1988) Development of the Colle-Salvetti correlation-energy formula into a functional of the electron-density. *Phys. Rev. B 37*, 785–789.
24. Stephens, P. J., Devlin, F. J., Chabalowski, C. F., and Frisch, M. J. (1994) Ab-initio calculation of vibrational absorption and circular-dichroism spectra using density-functional force-fields. *J. Phys. Chem. 98*, 11623–11627.
25. Jaguar 5.5 (2003) Schrodinger, LLC, Portland, OR.
26. Hay, P. J., and Wadt, W. R. (1985) Ab initio effective core potentials for molecular calculations. Potentials for K to Au including the outermost core orbitals. *J. Chem. Phys. 82*, 299–310.
27. Dunning, T. H. (1989) Gaussian basis sets for use in correlated molecular calculations. I. The atoms boron through neon and hydrogen. *J. Chem. Phys. 90*, 1007–1023.
28. Kendall, R. A., Dunning, T. H., and Harrison, R. J. (1992) Electron affinities of the first-row atoms revisited. Systematic basis sets and wave functions. *J. Chem. Phys. 96*, 6796–6806.
29. Woon, D. E., and Dunning, T. H. (1993) Gaussian basis sets for use in correlated molecular calculations. III. The atoms aluminum through argon. *J. Chem. Phys. 98*, 1358–1371.
30. Tannor, D. J., Marten, B., Murphy, R., Friesner, R. A., Sitkoff, D., Nicholls, A., Ringnalda, M., Goddard, W. A., and Honig, B. (1994) Accurate first principles calculation of molecular charge distributions and solvation energies from ab initio quantum mechanics and continuum dielectric theory. *J. Am. Chem. Soc. 116*, 11875–11882.
31. Marten, B., Kim, K., Cortis, C., Friesner, R. A., Murphy, R. B., Ringnalda, M. N., Sitkoff, D., and Honig, B. (1996) New model for calculation of solvation free energies: Correction of self-consistent reaction field continuum dielectric theory for short-range hydrogen-bonding effects. *J. Phys. Chem. 100*, 11775–11788.
32. Blomberg, M. R. A., Siegbahn, P. E. M., and Babcock, G. T. (1998) Modeling electron transfer in biochemistry: A quantum chemical study of charge separation in *Rhodobacter sphaeroides* and photosystem II. *J. Am. Chem. Soc. 120*, 8812–8824.
33. Jaguar version 7.0 (2007) Schrodinger, LLC, New York, NY.
34. Curtiss, L. A., Raghavachari, K., Redfern, P. C., and Pople, J. A. (2000) Assessment of Gaussian-3 and density functional theories for a larger experimental test set. *J. Chem. Phys. 112*, 7374–7383.

35. Siegbahn, P. E. M., and Blomberg, M. R. A. (1999) Density functional theory of biologically relevant metal centers. *Annu. Rev. Phys. Chem. 50*, 221–249.
36. Reiher, M., Salomon, O., and Hess, B. A. (2001) Reparameterization of hybrid functionals based on energy differences of states of different multiplicity. *Theor. Chem. Acc. 107*, 48–55.
37. Salomon, O., Reiher, M., and Hess, B. A. (2002) Assertion and validation of the performance of the B3LYP(star) functional for the first transition metal row and the G2 test set. *J. Chem. Phys. 117*, 4729–4737.
38. Roth, A., and Plass, W. (2008) Carboxylate-bridged dinuclear active sites in oxygenases: Diiron, dimanganese, or is heterodinuclear better? *Angew. Chem., Int. Ed. 47*, 7588–7591.
39. Bollinger, J. M., Chen, S. X., Parkin, S. E., Mangravite, L. M., Ley, B. A., Edmondson, D. E., and Huynh, B. H. (1997) Differential iron(II) affinity of the sites of the diiron cluster in protein R2 of *Escherichia coli* ribonucleotide reductase: Tracking the individual sites through the O-2 activation sequence. *J. Am. Chem. Soc. 119*, 5976–5977.
40. Willems, J. P., Lee, H. I., Burdi, D., Doan, P. E., Stubbe, J., and Hoffman, B. M. (1997) Identification of the protonated oxygenic ligands of ribonucleotide reductase intermediate X by Q-band H-1, H-2 CW and pulsed ENDOR. *J. Am. Chem. Soc. 119*, 9816–9824.
41. Han, W. G., Liu, T. Q., Lovell, T., and Noodleman, L. (2005) Active site structure of class I ribonucleotide reductase intermediate X: A density functional theory analysis of structure, energetics, and spectroscopy. *J. Am. Chem. Soc. 127*, 15778–15790.
42. Voevodskaya, N., Lendzian, F., Sanganas, O., Grundmeier, A., Gräslund, A., and Haumann, M. (2008) Redox intermediates of the Mn-Fe site in subunit R2 of *Chlamydia trachomatis* ribonucleotide reductase: An X-ray absorption and EPR study. *J. Biol. Chem.* (in press) (DOI:10.1074/jbc.M807190200).
43. Siegbahn, P. E. M. (2008) A structure-consistent mechanism for dioxygen formation in photosystem II (p NA). *Chem. Eur. J. 14*, 8290–8302.
44. Younker, J. M., Krest, C. M., Jiang, W., Krebs, C., Bollinger, J. M., and Green, M. T. (2008) Structural analysis of the Mn(IV)/Fe(III) cofactor of *Chlamydia trachomatis* ribonucleotide reductase by extended X-ray absorption fine structure spectroscopy and density functional theory calculations. *J. Am. Chem. Soc. 130*, 15022–15027.
45. Nordlund, P., and Eklund, H. (1993) Structure and function of the *Escherichia coli* ribonucleotide reductase protein R2. *J. Mol. Biol. 232*, 123–164.
46. Siegbahn, P. E. M. (2003) Mechanisms of metalloenzymes studied by quantum chemical methods. *Q. Rev. Biophys. 36*, 91–145.
47. Voegtli, W. C., Khidekel, N., Baldwin, J., Ley, B. A., Bollinger, J. M., and Rosenzweig, A. C. (2000) Crystal structure of the ribonucleotide reductase R2 mutant that accumulates a μ-1,2-peroxodiiron(III) intermediate during oxygen activation. *J. Am. Chem. Soc. 122*, 3255–3261.

BI801695D